Delft University of Technology

# Point spread function of photon-counting detectors under pile-up conditions
a proposed framework

Leibold, David; Van Der Sar, Stefan; Goorden, Marlies; Schaart, Dennis

**DOI**
10.1117/12.2612861

**Publication date**
2022

**Document Version**
Final published version

**Published in**
Progress in Biomedical Optics and Imaging - Proceedings of SPIE

**Citation (APA)**
Leibold, D., Van Der Sar, S., Goorden, M., & Schaart, D. (2022). Point spread function of photon-counting detectors under pile-up conditions: a proposed framework. *Progress in Biomedical Optics and Imaging - Proceedings of SPIE*, *12031*. https://doi.org/10.1117/12.2612861

**Important note**
To cite this publication, please use the final published version (if applicable).
Please check the document version above.

**Copyright**
Other than for strictly personal use, it is not permitted to download, forward or distribute the text or part of it, without the consent of the author(s) and/or copyright holder(s), unless the work is under an open content license such as Creative Commons.

**Takedown policy**
Please contact us and provide details if you believe this document breaches copyrights.
We will remove access to the work immediately and investigate your claim.

*This work is downloaded from Delft University of Technology.*
*For technical reasons the number of authors shown on this cover page is limited to a maximum of 10.*

***Green Open Access added to TU Delft Institutional Repository***

***'You share, we take care!' - Taverne project***

***https://www.openaccess.nl/en/you-share-we-take-care***

Otherwise as indicated in the copyright section: the publisher
is the copyright holder of this work and the author uses the
Dutch legislation to make this work public.

PROCEEDINGS OF SPIE

SPIEDigitalLibrary.org/conference-proceedings-of-spie

# Point spread function of photon-counting detectors under pile-up conditions: a proposed framework

Leibold, David, van der Sar, Stefan, Goorden, Marlies,
Schaart, Dennis

David Leibold, Stefan van der Sar, Marlies Goorden, Dennis Schaart, "Point spread function of photon-counting detectors under pile-up conditions: a proposed framework," Proc. SPIE 12031, Medical Imaging 2022: Physics of Medical Imaging, 120314R (4 April 2022); doi: 10.1117/12.2612861

Event: SPIE Medical Imaging, 2022, San Diego, California, United States

Downloaded From: https://www.spiedigitallibrary.org/conference-proceedings-of-spie on 10 Jun 2022 Terms of Use: https://www.spiedigitallibrary.org/terms-of-use

# Point Spread Function of Photon-Counting Detectors Under Pile-Up Conditions: A Proposed Framework

David Leibold[a], Stefan J. van der Sar[a], Marlies C. Goorden[a], Dennis R. Schaart[a,b]
[a] Department of Radiation Science and Technology, Delft University of Technology, Delft, The Netherlands
[b] Holland Proton Therapy Center, Delft, The Netherlands

## ABSTRACT

X-ray photon-counting detectors (PCDs) promise to revolutionise medical imaging. For an efficient comparison of detectors of various materials and with different setup choices, reliable detector performance measures are needed. The detector point spread function (PSF) is a commonly used measure, which describes the spatial response of a detector to the irradiation of a single pixel, given the energy spectrum of the source. In the case of an energy-resolving PCD, the detector PSF is typically derived for each energy bin and characterises its resolution. Moreover, it is commonly determined under low count rate conditions, to avoid dead time and pile-up related distortions. Under these assumptions, the PSF can be determined in a straightforward manner, but does not fully characterise the detector under all conditions encountered in clinical practice. This is especially true since the number of registered counts per energy bin depends on both the incident spectrum and the fluence rate, due to pile-up and dead time. We therefore propose a new metric, the differential point spread function (dPSF), which describes the change in the output count rate due to a small change in the input spectrum, for a given combination of incident spectrum and fluence rate. The dPSF can be used to characterise the spectral and spatial performance of a PCD under high fluence rate conditions, i.e., when its response becomes non-linear. We illustrate the use of the dPSF by performing a Monte-Carlo study in which we compare the response of direct-conversion and scintillation-based PCDs at different fluence rates.

**Keywords:** photon-counting detectors, X-ray detectors, pile-up, point spread function, energy response, medical imaging

## 1 INTRODUCTION

Photon-counting detectors (PCDs) herald the next leap in medical X-ray imaging, promising images with increased contrast-to-noise ratio, allowing for lower dose, and enabling multi-energy imaging capabilities[1–3], all of which could translate into substantial improvements in patient care. PCDs might prove to be a promising alternative to the currently dominant energy-integrating detectors (EIDs) in X-ray imaging. Whereas an EID only measures the total amount of energy deposited by X-rays in a single acquisition, a PCD is capable of resolving and counting the number of detector pulses generated by individual X-ray photons. Energy-resolving PCDs additionally assign each count to one of at least two energy bins, usually based on the pulse height, which is a measure of the energy deposited by the X-ray photon. In order to compare and optimise the performance of different PCDs, reliable detector performance measures are needed. In particular, performance measures that have been devised for energy-integrating detectors in the past may have to be adapted to be suitable for PCDs. In this work, we focus in particular on PCDs with energy-resolving capabilities.

A very important aspect of any imaging detector is the transfer of the spatial and/or spectral information in the incident beam by the detector. In this context, the detector point spread function (PSF) describes the detector's spatial response to the irradiation of a single point (*continuous PSF*) or pixel (*discretised PSF*) on its surface.[4] The PSF is a function of the physical properties of the detector (material, thickness, pixel size, etc.) and the energy of the incoming photons. For PCDs, the PSF should not only describe the spatial response of the detector (i.e., in which pixel energy is deposited), but also the spectral response (i.e., in which energy bin the count ends up).

An energy-integrating detector has a linear response, hence, the PSF for an incident beam with an arbitrary spectrum can always be expressed as a linear combination of PSFs of monoenergetic beams. The same is true for a PCD under low fluence rate conditions. However, in clinical practice photon counting detectors are exposed to very high fluence rates[5] of up to $3.5 \cdot 10^8$ mm$^{-2}$ s$^{-1}$. Under these circumstances, pile-up and dead time effects will affect the transfer of spatial and spectral information and the detector ceases to exhibit a linear response.

Medical Imaging 2022: Physics of Medical Imaging, edited by Wei Zhao, Lifeng Yu, Proc. of SPIE
Vol. 12031, 120314R · © 2022 SPIE · 1605-7422 · doi: 10.1117/12.2612861

Downloaded From: https://www.spiedigitallibrary.org/conference-proceedings-of-spie on 10 Jun 2022
Terms of Use: https://www.spiedigitallibrary.org/terms-of-use

*Pile-up* is due to two photons being absorbed in a single detector pixel shortly after each other. Since any detector has a finite response time, this may lead to incorrectly registered energies for one or both photons (in case they are still resolved as individual events) or to only a single count being registered (also with an incorrect energy). Furthermore, *dead time* refers to the finite time that the pixel readout needs to process a pulse, during which the detector is unable to process subsequent pulses. A PCD will hence incorrectly register the total number of photons, and, in case of an energy-resolving PCD, the number of photons per energy bin. The severity of this misregistration due to pile-up and dead time depends on the fluence rate, because a higher number of photons per second per detector pixel increases the pile-up probability as well as the likelihood that photons arrive within the detector's dead time.

In short, a comprehensive characterisation of PCDs should encompass its behaviour under high fluence rate conditions. The detector PSF, i.e., the probability for an incoming photon of a specific energy $E$ to end up in a certain energy bin $k$, then depends on both the fluence rate (which determines, e.g., the time difference between two photons that pile up) and the spectrum of the incoming beam (which determines, e.g., the energies of two photons that pile up).

The question is how to adapt the detector PSF such that it incorporates the dependency on the incident spectrum and fluence rate of a given acquisition. We start with adapting the notation by Persson et al.[6], who extended the description of linear detectors, such as EIDs, to PCDs with multiple energy bins. Let us first introduce a detector point spread function $h_k(\Delta\boldsymbol{n},E)$ that states the probability for photons of energy $E$, incident on the pixel $\boldsymbol{n}_0$, to be registered as a count in energy bin $k$ in pixel $\boldsymbol{n}$, with $\Delta\boldsymbol{n} = \boldsymbol{n} - \boldsymbol{n}_0$. Under the assumption that the system is linear and shift-invariant, and given an incoming spectrum $\phi$ (number of photons per energy and pixel $\boldsymbol{n}'$), we can now obtain the number of counts $d_k$ in pixel $\boldsymbol{n}$ and energy bin $k$ via the following convolution (Persson et al.[6], p. 4899, Eq. 1):

$$\overline{d_k}\,(\boldsymbol{n}) = \int_{\mathbb{R}^2} \int_0^{E_{\max}} h_k(\boldsymbol{n} - \boldsymbol{n}', E)\,\phi(\boldsymbol{n}', E)\,dE\,d\boldsymbol{n}' \tag{1}$$

Here, $h_k$ is the transfer function that describes how the spatial and spectral information is transformed by the detector.

As mentioned earlier, a PCD only behaves linear for low fluence rates of the incoming spectrum. In this regime, $h_k$ is independent of the fluence rate of the spectrum, which is why $\phi$ merely states the number of photons per energy and pixel, but not per unit time. As soon as the fluence rate of the incoming spectrum is large enough to cause a significant probability of pile-ups, the system is not linear anymore and the expression in Eq. 1 breaks down.

Developing a closed-form solution that relates the incoming spectrum at any given fluence rate to the number of counts $d_k$ appears to be a formidable task. In analogy to other non-linear systems, it might not be feasible to determine the function that relates the output (i.e., the count rate $d_k$) to the input (i.e., the spectral fluence rate). However, again using the analogy to other non-linear systems, we may investigate how the output of a PCD changes in response to small perturbations of the input (an approach referred to in electronics engineering as *small-signal modelling*).

We thus propose the *differential point spread function* (dPSF), denoted as $h_k'$. As indicated above, the dPSF is bound to the specific spectrum and fluence rate of a given acquisition, which we denote by $\dot{\Phi}(E')$ (number of incident photons per unit area, time and energy $E'$ in units of $\mathrm{mm}^{-2}\,\mathrm{s}^{-1}\,\mathrm{keV}^{-1}$) and call the *operating spectrum*. Accordingly, we include the dependency of the dPSF on the operating spectrum in its notation: $h_k'(\Delta\boldsymbol{n}, E, \dot{\Phi}(E'))$. The dPSF describes how a small change in the incident operating spectrum translates to a change in the counts registered by the detector. In other words, assuming that the detector is irradiated with a given operating spectrum, how does the resulting count rate (per pixel, unit time and energy bin) change if we superimpose a monoenergetic beam with energy $E$ and with a fluence rate low enough to not cause pile-ups between events of this monoenergetic beam?

It might help the readers' understanding to imagine how an experimental determination of $h_k'$ would be performed. One would start by irradiating the PCD uniformly with an operating spectrum of fluence rate $\dot{\Phi}(E')$. As a result, a given detector pixel $\boldsymbol{n}$ would register a count rate $d_k(\boldsymbol{n}, \dot{\Phi}(E'))$ in a given energy bin $k$ (note that we assume a shift-invariant detector, hence $d_k(\boldsymbol{n}, \dot{\Phi}(E'))$ is the same for all pixels). To determine the dPSF $h_k'(\Delta\boldsymbol{n}, E, \dot{\Phi}(E'))$, a *single* pixel $\boldsymbol{n}_0$ is then additionally irradiated with a monoenergetic probe beam of energy $E$ and fluence rate $\dot{\Phi}_E^{\boldsymbol{n}_0}$, where the fluence rate $\dot{\Phi}_E^{\boldsymbol{n}_0}$ is chosen such that the likelihood of pile-up between events of this monoenergetic beam is negligible. After measuring the registered count rate $d_k(\boldsymbol{n}, \dot{\Phi}(E') + \dot{\Phi}_E^{\boldsymbol{n}_0})$ for all $\boldsymbol{n}$ and $k$, the dPSF is simply calculated as the difference in count rate in each of the pixels and energy bins before and after adding the monoenergetic probe beam in pixel $\boldsymbol{n}_0$, normalised by the total number of photons in the probe beam per unit time, $N_{\dot{\Phi}_E^{\boldsymbol{n}_0}}$:

Downloaded From: https://www.spiedigitallibrary.org/conference-proceedings-of-spie on 10 Jun 2022
Terms of Use: https://www.spiedigitallibrary.org/terms-of-use

$$h_k{}'(\Delta\boldsymbol{n}, E, \dot{\Phi}(E')) \; = \; \frac{d_k(\boldsymbol{n},\dot{\Phi}(E')+\dot{\Phi}_E^{\boldsymbol{n}_0}) - d_k(\boldsymbol{n},\dot{\Phi}(E'))}{N_{\dot{\Phi}_E^{\boldsymbol{n}_0}}} \tag{2}$$

In this study, we determine the dPSF by means of a Monte-Carlo (MC) simulation and investigate the influence of the fluence rate of a given spectrum on the detector response. In the MC simulation we use a monoenergetic probe beam, sweeping its energy across the energy range of interest, and using a near-continuous energy binning. This approach facilitates obtaining a detailed insight into the effects at play.

For the detector types and materials, we chose to compare direct-conversion and indirect-conversion PCDs. While the realisation of PCDs for medical imaging largely focuses on direct-conversion detectors based on CdTe or CdZnTe (CZT), the cost-effective synthesis of detector-grade material remains challenging. Indirect-conversion, scintillation-based PCDs may combine cost-effective growth of detector-grade material with efficient X-ray absorption, which is why we are investigating silicon photomultiplier (SiPM)-based scintillation detectors as an alternative.[7] In this simulation study, we compare a direct-conversion detector based on CZT with a scintillation detector based on $LaBr_3$:Ce.

# 2 MATERIALS AND METHODS

## 2.1 Monte-Carlo simulation

A Monte-Carlo (MC) simulation was implemented based on the GATE MC software[8] (version 9.0), which utilises the GEANT4 toolkit[9] (version 10.6.2). It simulates the irradiation of a detector with X-rays of a given spectrum (see section **X-ray spectra**) and outputs for each incident photon in which pixels energy is deposited as well as how much energy is deposited there. We refer to such an energy deposition in a pixel as an *event* in this work. The simulated events were subsequently processed with a pulse train analysis to mimic a PCD (see section **Pulse train analysis**).

For comparison, two detectors are considered: a $LaBr_3$:Ce scintillation crystal coupled to a silicon photomultiplier, and a CZT-based direct-conversion detector. It is noted that we do not include optical photon transport and charge sharing in the simulations. The absorbing layer of the direct-conversion detector consists of 2 mm thick CZT, while 2.9 mm thick $LaBr_3$:Ce(5%) is used in the scintillation-based detector. This thickness of $LaBr_3$:Ce achieves the same X-ray attenuation as 2 mm thick CZT, averaged over the incident spectrum of a 120 kVp source having passed through 200 mm water.

The pixel pitch was set to 500 μm for both setups; in order to account for a smaller active pixel size due to a reflective coating of the scintillation crystals, a 65 μm thick enhanced specular reflector (ESR) foil was included, which is wrapped around each pixel and reduces the effective pixel size by 65 μm, while keeping the pixel pitch at a value of 500 μm. We could not find specific information on the composition of the ESR films other than that they consist of polyester. Therefore, we implemented ESR as the polyester polyethylene terephthalate (PET, $(C_{10}H_8O_4)_n$) in the MC simulation.

CZT was defined as $Cd_{0.9}Zn_{0.1}Te$ and a density of 5.68 $g/cm^3$. $LaBr_3$:Ce(5%) was defined with a 1:3 ratio between La and Br, where 5% of the La ions are replaced by Ce; the density was set to 5.29 $g/cm^3$.

The physics model used by the MC simulation was based on the *emstandard_opt4* option in GATE. X-ray fluorescence was enabled by setting the range cut to 10 μm for photons and to 1000 μm for electrons. The remaining physics settings were kept at their default values. All events were registered and stored in GATE, without rejecting events below a certain energy threshold.

In order to reduce computation time in the MC simulation, only the centre pixel of a pixel array was irradiated with the operating spectrum. Summing up the events registered in all pixels (centre and neighbouring pixels) and assigning them all to one pixel mimics the situation that the whole pixel array is illuminated homogeneously, including inter-pixel crosstalk. However, there is one caveat: imagine that an X-ray photon undergoes Compton-scatter in the centre pixel, depositing part of its energy, and subsequently is absorbed via photoelectric absorption in a neighbouring pixel, depositing the remaining energy. The time interval between the two events would be too small to be resolved by the detector. If we simply added up the event from the neighbouring pixel to the event in the centre pixel, they would appear as a single event in the resulting pulse train with the full energy of the incident photon, and therefore no spectral degradation is observed. This is in contrast to a real device that is homogeneously illuminated, where there is no correlation between time stamps of primary interactions in a certain pixel and higher-order interaction events originating from primary interactions in

Downloaded From: https://www.spiedigitallibrary.org/conference-proceedings-of-spie on 10 Jun 2022
Terms of Use: https://www.spiedigitallibrary.org/terms-of-use

neighbouring pixels. To account for this, we randomly shifted the time stamps of all pixels in the simulated pixel array before combining all events together into one pixel.

### 2.2 X-ray operating spectrum

We used a water phantom to create a clinically realistic operating spectrum. The emission spectrum of an X-ray tube was obtained from SpekCalc[10] and is based on a tungsten source, filtered by 10 mm aluminium, and 140 kVp source voltage. In Gate, this X-ray spectrum was passed through a 200 mm thick water cylinder of 500 mm diameter, with the cylinder's base facing the source. At a distance of 600 mm from the centre of the disk, the X-rays passing through the water phantom were registered by a circular area of 500 mm diameter.

### 2.3 Pulse train analysis

For a given set of simulated events of energy $E_i$ with time stamps $t_i$ (sampled with 1 ns resolution), the generated pulse train is a convolution of a delta pulse train, i.e., $\Sigma_i E_i \cdot \delta(t - t_{i,})$, with a pulse shape function $p(t)$. Prior to this convolution, an energy blurring was applied to model the finite energy resolution of the system, which was set to 12.5 % FWHM at 59.5 keV for the scintillation detector (expected value based on the model presented by van der Sar et al.[7]) and to 8.0 % FWHM at 59.5 keV for the direct-conversion detector[11]. The energy dependence of the FWHM energy resolution was modelled as an inverse square law behaviour.

For the $LaBr_3$:Ce detector, the applied pulse shape $p(t)$ is the convolution of two exponentially decaying functions with infinitesimal rise time, to model both the scintillation decay and the response of the SiPM. The two decay time constants are 16 ns for $LaBr_3$:Ce [12] and 7 ns for the SiPM. For the CZT detector a Gaussian pulse shape with a FWHM of 20 ns [11] was chosen.

### 2.4 Counting mode

After a pulse in the pulse train triggers the PCD by rising above a pre-defined threshold, a count is registered and an analysis window of length $\tau$ starts. The maximum signal within this window is taken as the energy associated with the count. In this study, we implemented a non-paralysable-like counting mode. This means that if the signal is still above the threshold at the end of the analysis window of length $\tau$, a new count is immediately registered and a new analysis window starts in which the energy is determined, and so on. If the signal is no longer above the threshold at the end of an analysis window, the next count is registered when the pulse train crosses the threshold again.

The trigger threshold was set to 20 keV and the energy bins for the registered counts had a width of 1 keV, with the lowest bin edge at 20 keV and the highest at 251 keV. Any registered count with an energy exceeding 251 keV was assigned to the uppermost bin. The length $\tau$ of the analysis window was chosen such that 95% of the area under the pulse falls within $\tau$. This translates into $\tau = 58$ ns for the $LaBr_3$:Ce detector, and $\tau = 34$ ns for the CZT detector.

## 3 RESULTS AND DISCUSSION

As elaborated previously, the dPSF relates a pertubation in the incident spectral fluence rate $\dot{\Phi}(E')$ to the corresponding change in detector output (i.e., counts $d_k$ per pixel and energy bin). Due to the non-linearity of a PCD under high pile-up conditions, the dPSF depends on the given operating spectrum and fluence rate. For our analysis, we use the spectrum of an X-ray tube with a tungsten target, operated at 140 kVp, passing through 200 mm water (see **Methods and Materials** section) as our operating spectrum $\dot{\Phi}$. We chose a maximum fluence rate for the operating spectrum of $4 \cdot 10^7$ mm$^{-2}$ s$^{-1}$ (integrated over all energies), which covers, depending on the patient size, 95 % of the observed fluence rates in the detector pixels behind the patient during a chest scan[5]. We then vary the fluence rate of the operating spectrum between zero and the aforementioned maximum fluence rate and determine $h_k'$ in each case.

Note that, in the case of zero fluence rate of the operating spectrum, we are left with just the monoenergetic probe beam with fluence rate $\dot{\Phi}_E^{n_0}$, which is chosen low enough to keep the likelihood of pile-up between probe beam events negligible. The only spectral degradation is now caused by crosstalk and by the limited energy resolution of the detector, which leads

Downloaded From: https://www.spiedigitallibrary.org/conference-proceedings-of-spie on 10 Jun 2022
Terms of Use: https://www.spiedigitallibrary.org/terms-of-use

to some events still being registered above the peak voltage of the X-ray tube. In this limit of zero fluence rate of the operating spectrum, the PCD operates in the linear regime and $h_k'$ is equivalent to the PSF of the monoenergetic probe beam(s).

Figure 1 shows $h_k'$ under the given operating spectrum and for various fluence rates, for both the simulated LaBr$_3$ and CZT detectors. While we simulated two-dimensional detector arrays, the plots only show a cross-section of the discrete dPSFs along a single line of pixels, including the pixel $\boldsymbol{n}_0$, and along all registered energy bins. For reasons of brevity, we limit ourselves to $h_k'$ integrated over all incident energies $E$ of the monoenergetic probe beams, that is, $\int_{20\,keV}^{150\text{ keV}} h_k'(\Delta\boldsymbol{n}, E, \dot{\Phi}(E'))\, dE = h_k'(\Delta\boldsymbol{n}, \dot{\Phi}(E'))$. The result is equivalent to adding a probe beam with a continuous, white spectrum between 20 and 150 keV, i.e., photons from all energies are equally likely, on top of the operating spectrum. Again, the fluence rate in the probe beam is low enough to prevent pile-up. In this case the plots of $h_k'$ in Figure 1 provide a way to visualise the resulting change in the output count rate for each energy bin, which allows to assess both the spectral and spatial degradation of the detector performance in an intuitive way. To derive the response that a real PCD with only a limited number of energy bins would yield to this white spectrum, one would additionally integrate over the registered energies that are covered by each of the energy bins of this real PCD.

The left column of Figure 1 presents $h_k'$ for the LaBr$_3$:Ce detector (1a, c and e), and the right column for the CZT detector (1b, d, and f). The first two rows are the result of a homogeneous illumination by the operating spectrum at fluence rates of $4 \cdot 10^7$ mm$^{-2}$ s$^{-1}$ (a, b) and $4 \cdot 10^6$ mm$^{-2}$ s$^{-1}$ (c, d), respectively. The last row (1e and f) presents the result in case of an absent operating spectrum.

Starting at the case of zero fluence rate (Fig. 1e and f), we can clearly see that the dPSFs in LaBr$_3$ have a larger spatial extent than in CZT. In other words, changing the incident spectrum in the centre pixel slightly has ramifications over a larger area in LaBr$_3$ compared to CZT. This is due to the difference in attenuation coefficients: in the energy range between 20 and 150 keV, the mass attenuation coefficient of LaBr$_3$ is on average 18 % lower than that of CZT. Furthermore, the prominent features in the low energy range (below 40 keV) are due to X-ray fluorescence and K-escape photons registered in neighbouring pixels. This means, that a small change in the incoming spectrum very likely causes a change in the energy bins associated with X-ray fluorescence and K-escape.

Adding an operating spectrum (Fig. 1a-d), the events caused by photons of the monoenergetic probe beams will pile-up with events caused by the operating spectrum, and are hence registered in higher energy bins. This leads to $h_k'$ being stretched to higher energy bins; the larger the fluence rate of the operating spectrum, the more $h_k'$ extends to higher energies. Due to severe pile-up under higher fluence rates, a pertubation of a single energy of the operating spectrum can have an effect on the number of registered counts in more energy bins than without pile-up.

The dPSF provides insights into how the information in the image is preserved at different fluence rates. Let us first consider two limits of detector operation, that is, the case of a near-zero operating spectrum and the case of nearly complete saturation of the detector. In the first case, i.e., near-zero operating spectrum, a PCD with its given physical properties maximises the transfer of information, since no events are lost due to dead time and no events are registered in the incorrect energy bin due to pile-up. In the second case, i.e., nearly complete detector saturation, the information is spread over the full energy range in conjunction with a severe loss of counts.

Hence, $h_k$' allows insights into how the PCD, given an operating spectrum and fluence rate, preserves information content. This closely relates to imaging tasks such as lesion detection, which presents as a small change in the operating spectrum for a given voxel in the object to be scanned. The pertubation in the operating spectrum due to the lesion should result into a well-defined change of count rate in order to enable optimal detection in the reconstructed images.

It is worth pointing out that $h_k'$ in Figures 1a and 1b also exhibits negative numbers. Although negative values for a measure related to the PSF may seem counter-intuitive at first sight, it can readily be explained: the events caused by a monoenergetic probe beam can pile-up with the events created by the operating spectrum; subsequently, the events of the operating spectrum will be registered at higher energies and are therefore removed from the lower energy part of the operating spectrum. In other words, adding a small number of X-ray photons to the operating spectrum decreases the count rates in the low energy bins.

To further the understanding of $h_k'$, Figure 2a shows a slice of $h_k'$ for a monoenergetic probe beam of 100 keV incident on the centre pixel $\boldsymbol{n}_0$ of the LaBr$_3$ detector. The figure hence shows how a photon of 100 keV, incident on the centre pixel $\boldsymbol{n}_0$, alters the counts in any of the given energy bins. $h_k'$ is shown in case of an operating spectrum with fluence rates $4 \cdot 10^7$ mm$^{-2}$ s$^{-1}$ and $2 \cdot 10^7$ mm$^{-2}$ s$^{-1}$, as well as in the case of no operating spectrum. Please note that in contrast to Figure 1,

Downloaded From: https://www.spiedigitallibrary.org/conference-proceedings-of-spie on 10 Jun 2022
Terms of Use: https://www.spiedigitallibrary.org/terms-of-use

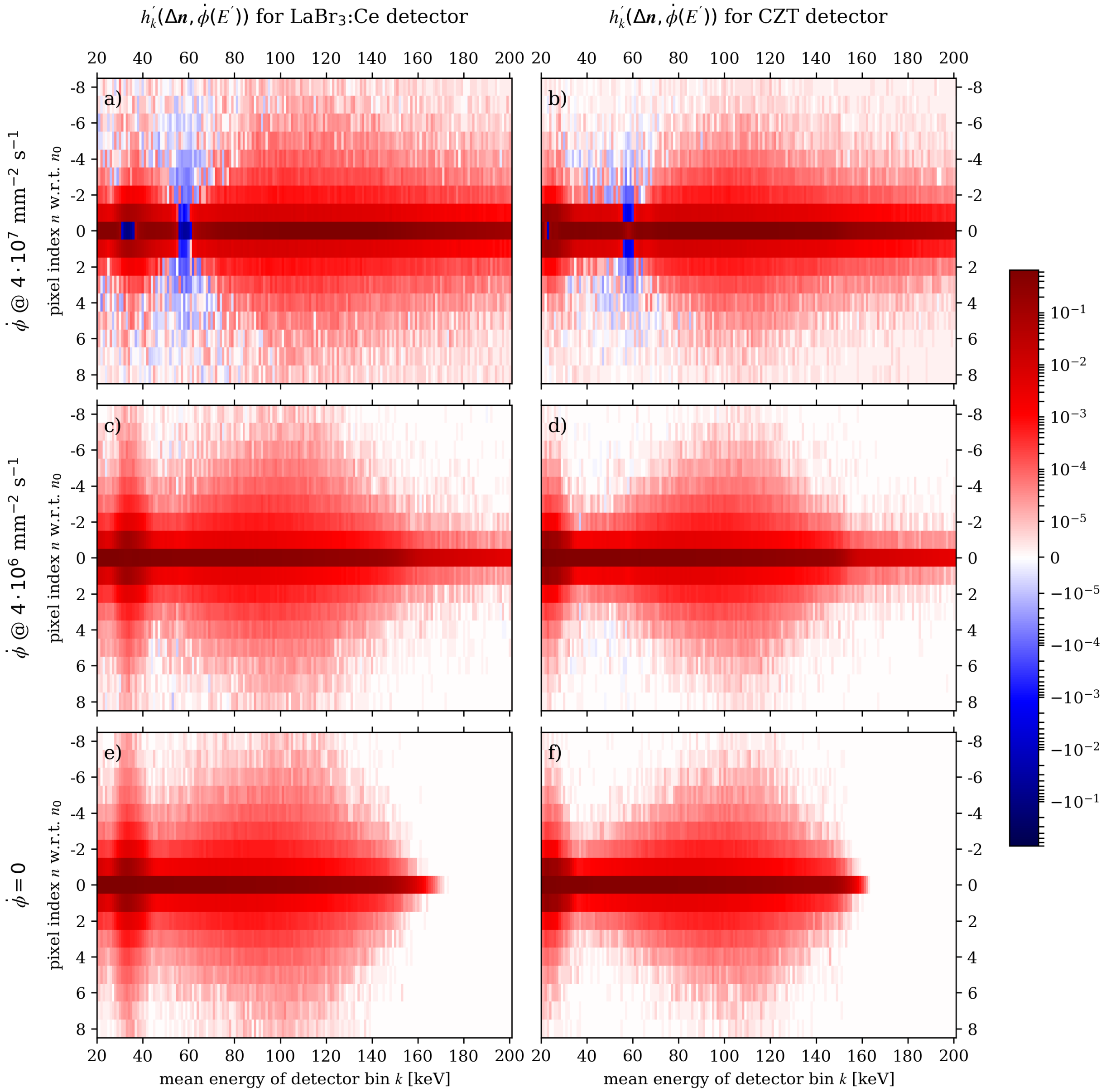

Figure 1: Slice of the differential point spread function $h_k'(\Delta \boldsymbol{n}, \dot{\Phi}(E'))$ along the pixel axis over the registered energy bins $k$ (width of 1 keV), integrated over all incident energies from 20 to 150 keV and under homogeneous illumination of an operating spectrum $\dot{\Phi}(E')$. Two detector setups are considered, LaBr$_3$:Ce (left column, a, c, e) and CZT (right column, b, d, f). The top row (a, b) assumes a fluence rate of $4 \cdot 10^7$ mm$^{-2}$ s$^{-1}$, while the middle row (c, d) pertains to a fluence rate of $4 \cdot 10^6$ mm$^{-2}$ s$^{-1}$, and the bottom row (e, f) shows the result in the limit of zero fluence rate. The operating spectrum $\dot{\Phi}(E')$ is based on the spectrum of a 140 kVp X-ray source after passing through 200 mm water; the pixel pitch for both detectors is 500 µm.

Figure 2 shows $h_k'$ for a single incident energy only. A comparison between the cases with and without an operating spectrum clearly shows how the events are removed from the lower energy part of the spectrum and are instead registered, due to pile-up, in bins of higher energy.

Attentive readers might have noticed that in Fig. 2a the K-escape peak, located 39 keV below the energy of the incident beam (100 keV), is clearly visible, while no peak of K-fluorescence events is present at 39 keV. This is because $h_k'$ states the change in counts in a specific pixel (in this case, the centre pixel $\boldsymbol{n}_0$) and a specific energy bin if a photon with incident

Downloaded From: https://www.spiedigitallibrary.org/conference-proceedings-of-spie on 10 Jun 2022
Terms of Use: https://www.spiedigitallibrary.org/terms-of-use

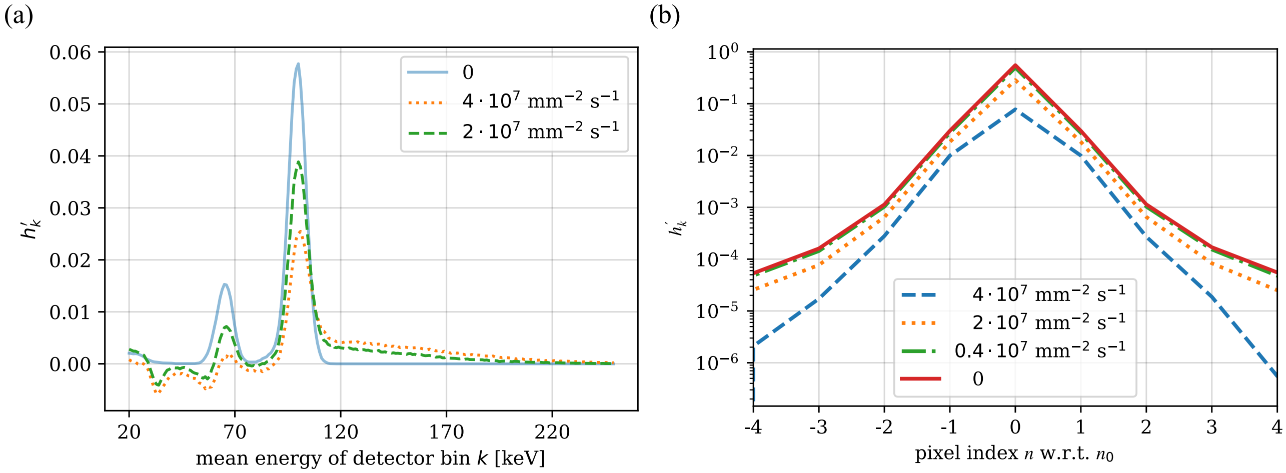

Figure 2: a) A slice of $h_k'$ along all registered energy bins in the centre pixel $\boldsymbol{n}_0$ of the LaBr$_3$:Ce detector, based on an incident energy of 100 keV. The figure compares different fluence rates of the operating spectrum, and also the edge case of no operating spectrum being present. b) A slice of $h_k'$ of the simulated LaBr$_3$:Ce detector along the pixel axis, summed over all incident energies, and summed over the registered energy bins from 20 to 60 keV. The figure compares different fluence rates of the operating spectrum, and also the edge case of no operating spectrum being present. The operating spectrum is based on a 140 kVp X-ray source and a 200 mm thick water phantom.

energy of 100 keV is added to the operating spectrum. If there are K-escape events, then they will be registered in neighbouring pixels, hence these are not registered in the pixel of the incident probe beam.

Figure 2b depicts the response of the LaBr$_3$ detector under an operating spectrum with fluence rates of 0, 0.4, 2 and $4 \cdot 10^7$ mm$^{-2}$ s$^{-1}$. It shows $h_k'$ for a slice around the centre pixel $\boldsymbol{n}_0$, summed over all incident energies and over all registered energy bins from 20 to 60 keV. This mimics a low-energy bin in a real PCD with only a limited number of energy thresholds available. Again, the result shows that with increasing fluence rate, counts are removed from the lower energy part of the spectrum and hence this low energy bin.

## 4 CONCLUSIONS

In this work, we study the dependence of the point spread function of photon-counting detectors on the incident spectrum and fluence rate, with the aim to establish a framework for characterising PCDs under increased pile-up and dead time conditions, i.e., when their response becomes non-linear. This may help to assess the performance of photon-counting systems under clinically realistic operating conditions. Furthermore, it may enable the extension of comprehensive characterisation frameworks, such as presented by Persson et al.[6], to scenarios that are not limited to low fluence rates. We introduce a differential point spread function (dPSF) $h_k'$, which relates a perturbation in the incident operating spectrum to the corresponding change in registered counts per pixel and energy bin. We applied the proposed formalism via a MC simulation on two X-ray detector setups, a direct-conversion CZT detector as well as a LaBr$_3$:Ce scintillation detector. Our results show that the dPSF characterises the transfer of information in a PCD, which is increasingly impeded when the fluence rate of the operating spectrum increases. This proves that a comprehensive characterisation of PCDs requires the quantification of their response beyond the limit of zero fluence rate.

*This work is not being, or has not been, submitted for publication or presentation elsewhere.*

## ACKNOWLEDGEMENTS

This research was partially funded by Varian, a Siemens Healthineers Company, grant number 2018016.

Downloaded From: https://www.spiedigitallibrary.org/conference-proceedings-of-spie on 10 Jun 2022
Terms of Use: https://www.spiedigitallibrary.org/terms-of-use

## REFERENCES

[1] Willemink, M. J., Persson, M., Pourmorteza, A., Pelc, N. J. and Fleischmann, D., "Photon-counting CT: Technical Principles and Clinical Prospects," Radiology **289**(2), 293–312 (2018).

[2] Flohr, T., Petersilka, M., Henning, A., Ulzheimer, S., Ferda, J. and Schmidt, B., "Photon-counting CT review," Physica Medica **79**, 126–136 (2020).

[3] Danielsson, M., Persson, M. and Sjölin, M., "Photon-counting x-ray detectors for CT," Phys. Med. Biol. **66**(3), 03TR01 (2021).

[4] Barrett, H. H. and Myers, K. J., [Foundations of image science], Wiley-Interscience, Hoboken, NJ (2004).

[5] Persson, M., Bujila, R., Nowik, P., Andersson, H., Kull, L., Andersson, J., Bornefalk, H. and Danielsson, M., "Upper limits of the photon fluence rate on CT detectors: Case study on a commercial scanner," Medical Physics **43**(7), 4398–4411 (2016).

[6] Persson, M., Rajbhandary, P. L. and Pelc, N. J., "A framework for performance characterization of energy-resolving photon-counting detectors," Med. Phys. **45**(11), 4897–4915 (2018).

[7] van der Sar, S. J., Brunner, S. E. and Schaart, D. R., "Silicon photomultiplier-based scintillation detectors for photon-counting CT: A feasibility study," Med. Phys., mp.14886 (2021).

[8] Sarrut, D., Bardiès, M., Boussion, N., Freud, N., Jan, S., Létang, J.-M., Loudos, G., Maigne, L., Marcatili, S., Mauxion, T., Papadimitroulas, P., Perrot, Y., Pietrzyk, U., Robert, C., Schaart, D. R., Visvikis, D. and Buvat, I., "A review of the use and potential of the GATE Monte Carlo simulation code for radiation therapy and dosimetry applications: GATE for dosimetry," Med. Phys. **41**(6Part1), 064301 (2014).

[9] Allison, J., Amako, K., Apostolakis, J., Arce, P., Asai, M., Aso, T., et al., "Recent developments in Geant4," Nuclear Instruments and Methods in Physics Research Section A: Accelerators, Spectrometers, Detectors and Associated Equipment **835**, 186–225 (2016).

[10] Poludniowski, G., Landry, G., DeBlois, F., Evans, P. M. and Verhaegen, F., "SpekCalc: a program to calculate photon spectra from tungsten anode x-ray tubes," Physics in Medicine and Biology **54**(19), N433–N438 (2009).

[11] Steadman, R., Herrmann, C., Mülhens, O. and Maeding, D. G., "ChromAIX: Fast photon-counting ASIC for Spectral Computed Tomography," Nuclear Instruments and Methods in Physics Research Section A: Accelerators, Spectrometers, Detectors and Associated Equipment **648**, S211–S215 (2011).

[12] Lecoq, P., "Development of new scintillators for medical applications," Nuclear Instruments and Methods in Physics Research Section A: Accelerators, Spectrometers, Detectors and Associated Equipment **809**, 130–139 (2016).

Downloaded From: https://www.spiedigitallibrary.org/conference-proceedings-of-spie on 10 Jun 2022
Terms of Use: https://www.spiedigitallibrary.org/terms-of-use